Available online at www.sciencedirect.com

ScienceDirect

Procedia Structural Integrity 2 (2016) 573–580

Structural Integrity Procedia

www.elsevier.com/locate/procedia

21st European Conference on Fracture, ECF21, 20-24 June 2016, Catania, Italy

Effect of corrosion-induced hydrogen embrittlement and its degradation impact on tensile properties and fracture toughness of (Al-Cu-Mg) 2024 alloy

Nikolaos D. Alexopoulos[a,*], Wolfgang Dietzel[b]

[a]*Department of Financial Engineering, University of the Aegean, 82 132 Chios, Greece*
[b]*Institute of Materials Research, Department of Corrosion and Surface Technology, Helmholtz-Zentrum Geesthacht, Max-Planck-Straße 1, 21502 Geesthacht, Germany*

Abstract

In the present work, the effect of artificial ageing of AA2024-T3 on the tensile mechanical properties and fracture toughness degradation due to corrosion exposure will be investigated. Tensile and fracture toughness specimens were artificially aged to tempers that correspond to Under-Ageing (UA), Peak-Ageing (PA) and Over-Ageing (OA) conditions and then were subsequently exposed to exfoliation corrosion environment. The corrosion exposure time was selected to be the least possible according to the experimental work of Alexopoulos et al. (2016) so as to avoid the formation of large surface pits, trying to simulate the hydrogen embrittlement degradation only. The mechanical test results show that minimum corrosion-induced decrease in elongation at fracture was achieved for the peak-ageing condition, while maximum was noticed at the under-ageing and over-ageing conditions. Yield stress decrease due to corrosion is less sensitive to tempering; fracture toughness decrease was sensitive to ageing heat treatment thus proving that the S' particles play a significant role on the corrosion-induced degradation.

Peer-review under responsibility of the Scientific Committee of ECF21.

Keywords: alloy 2024; tension; fracture toughness; artificial ageing; exfoliation corrosion; ductility

* Corresponding author. Tel.: +0030-22710-35464; fax: +0030-22710-35429.
E-mail address: nalexop@aegean.gr

Copyright © 2016 The Authors. Published by Elsevier B.V. This is an open access article under the CC BY-NC-ND license (http://creativecommons.org/licenses/by-nc-nd/4.0/).
Peer review under responsibility of the Scientific Committee of ECF21.
10.1016/j.prostr.2016.06.074

1. Introduction

Aluminum alloy 2024 is a high strength alloy with a complex microstructure, comprising the aluminum matrix as well as a number of different intermetallic particles. Several articles tried to characterize the resulting microstructure of the alloy and the respective composition of the intermetallic particles, e.g. Buchheit et al. (1997) and Boag et al. (2007). It is well known that AA2024 is strengthened by microstructure evolution (precipitates) during ageing. Bagaryatsky (1952) proposed the following precipitation sequence *SSS* → *GPB zone* → *S″* → *S′* → *S*, where *SSS* stands for supersaturated solid solution and *GPB* stands for Guinier-Preston-Bagaryatsky; *GPB* is considered to be a short range ordering of Cu and Mg solute atoms while *S″* are very small precipitates fully coherent with the Al matrix. The *S* phase is an equilibrium phase and is incoherent with the Al matrix. Mondolfo (1976) considers the *S′* phase as semi-coherent with the matrix, having the same structure as the *S*-phase but with slightly different lattice parameters. Ringer et al. (1996) and (1998) confirmed that *GPB* zones and other precipitate-structures prior to the *S*-phase formation are the dominant precipitates at the strengthening regime of the ageing curve, while the *S*-phase appears in the softening regime (over-ageing condition).

In order to investigate the hydrogen embrittlement effect, a wide variety of methods to introduce hydrogen has been used over the years, such as cathodic charging investigated by Larignon et al (2013), exposure to humid air as well as exposure to a corrosive environment. For the latter case, it is quite often the degradation mechanism to be a synergy of stress-concentration induced by the corrosion-induced surface pits and subsequent micro-cracking as well as of hydrogen embrittlement. For example, Alexopoulos and Papanikos (2008) showed that the total reduction of almost 30 % of the fracture toughness of AA2024-T3 after 96 h exposure to exfoliation corrosion solution was attributed primary to the reduction of the alloy effective thickness (22 %) and secondary to the hydrogen embrittlement (8 %) mechanism. Hence, in order to assess the true hydrogen embrittlement effect, short exposure times should be selected to corrode the specimens so as to prevent the formation of corrosion-induced surface pits that act as stress raisers and degrade the ductility of the alloy. The corrosion exposure time was experimentally derived to be 2 hours, as according to Alexopoulos et al. (2016) it was the least possible so as to avoid the formation of large surface pits, trying to simulate the hydrogen embrittlement phenomenon only.

2. Materials and experimental procedure

The material used for the present investigation was AA2024 wrought aluminum alloys that were received in sheet form with nominal thickness of 3.2 mm. The weight percentage chemical composition of the alloy is 0.50% Si, 0.50% Fe, 4.35% Cu, 0.64% Mn, 1.50% Mg, 0.10% Cr, 0.25% Zn, 0.15% Ti and Al rem. Tensile and fracture toughness specimens were machined from the longitudinal (L) direction of the material according to ASTM E8 and E561 specifications, respectively. Prior to corrosive solution exposure, all surfaces of the specimens were cleaned with alcohol according to ASTM G1 specification.

All specimens were isothermally artificially aged (heat treated) in an electric oven with air circulation Elvem (2600 W) with ± 0.1ºC temperature control. Artificial ageing conditions were performed at 190ºC and for different ageing times. Ageing times were selected to correspond to all ageing conditions, including Under-Ageing (UA), Peak-Ageing (PA) and Over-Ageing (OA). Immediately after the artificial ageing, half of the specimens were immediately tested while the rest were surfaced cleaned according to ASTM G34 and then exposed to the laboratory exfoliation corrosion environment (hereafter called EXCO solution) according to the specification ASTM G34. The corrosive solution consisted of the following chemicals diluted in 1 l distilled water; sodium chloride (4.0M NaCl), potassium nitrate (0.5 KNO_3) and nitric acid (0.1 M HNO_3). More details can be seen in the respective specification. The corrosion exposure was selected according to Alexopoulos et al. (2016) to be 2 h so as to have the least pitting formation and hence, any ductility decrease to be attributed to the hydrogen embrittlement effect and not to the corrosion-induced surface notches. After the corrosion exposure, the corroded specimens were immediately cleaned according to the same specification and then mechanically tested.

Tensile and fracture toughness tests were carried out in servo-hydraulic Instron 100 kN testing machine according to ASTM E8 and E561 specifications, respectively. For the tensile tests an external extensometer was attached at the reduced cross-section gauge length of specimen, while for the fracture toughness tests a crack mouth opening displacement (CMOD) was attached at the mouth of the notch. Three specimens were tested in each

different case to get reliable average data. A data logger was used during all the experiments and the values of load, displacement, axial strain or CMOD readings were recorded and stored in a computer.

3. Results and discussion

One of the main goals of the present article is to investigate and compare the mechanical behavior of AA2024 for various artificial ageing conditions after being exposed to the common 2 h exposure to the corrosive solution. Typical engineering stress - strain tensile flow curves can be seen in Fig. 1a for different artificial ageing times at 190ºC ageing temperature. It is evident that the different artificial ageing conditions have an essential effect on the stress - strain flow curves. Yield stress and ultimate tensile strength are increasing with increasing ageing time up to a maximum up till 9 hours, while an essential decrease in ductility is noticed. For longer ageing times (over-ageing condition), a gradual decrease in yield stress is noticed while ductility seems not to be essentially recovered at high ageing conditions.

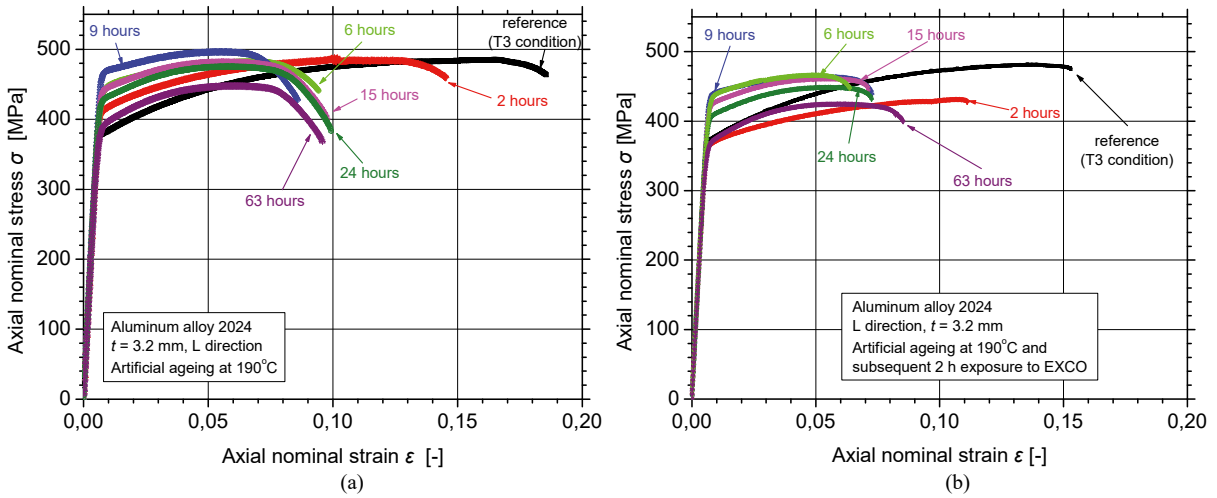

Fig. 1. Typical experimental tensile flow curves of artificially aged aluminum alloy 2024 tensile specimens (a) without; (b) with pre-corrosion for 2 h exposure time to the exfoliation corrosion solution.

Fig. 1b shows the respective tensile flow curves for the artificially aged tensile specimens when subsequently exposed to the corrosion solution and then tensile tested. It is evident that the corrosion exposure decreases all the tensile mechanical properties, including strength and ductility capability of the specimens. This decrease seems to be ageing condition dependent and the corrosion effect on each mechanical property will be discussed in detail in the following section.

Typical experimental force –crack opening displacement (COD) curves, hereafter called as resistance curves, can be seen in Fig. 2a for the different artificial aging times at 190ºC of AA2024. As expected, the resistance curve of the alloy becomes more compliant with the increase of artificial aging time. This means that the maximum applied force P_{max} decreases and the value of the COD at the maximum force also decreases with the ageing time increase. Fig. 2b shows the respective curves of the specimens having the same aging conditions and subsequent 2 h exposure to exfoliation corrosion solution. It is evident that the corrosion exposure affects the resistance curves of the specimens and in the following the fracture toughness decrease will be quantitatively assessed.

3.1. Effect on mechanical properties

3.1.1. Conventional yield stress

Conventional yield stress $R_{p0.2\%}$ was calculated based on the nominal cross-section of the tensile specimens. The non-artificially aged material exhibited 387 MPa yield stress while after 2 hours exposure its yield stress was

decreased by approximately 5.6 % (365 MPa). For higher artificial ageing times, the effect of corrosion exposure seems to result to a slightly higher decrease on yield stress; the $R_{p0.2\%}$ decrease due to corrosion is almost minimal at the latest stages of under-ageing, it increases marginally up to 8.6 % at the peak-ageing and ends at the same order of magnitude (5.3 % decrease) for the case of over-ageing conditions.

Peak strength can be achieved due to the well-balanced formation of coherent and sub-sequent non-coherent S'' and S' (Al_2CuMg) precipitates, respectively according to Mondolfo (1976). From peak-ageing and after, no more S'' second phase is being precipitated, while growth of the precipitates is observed, that leads to larger precipitates and fewer in number. Yield stress degradation due to the small 2 h exposure time to the corrosion solution is also noticed for all ageing times; for all ageing conditions this decrease seems to be constant and approximately around 5.7 %.

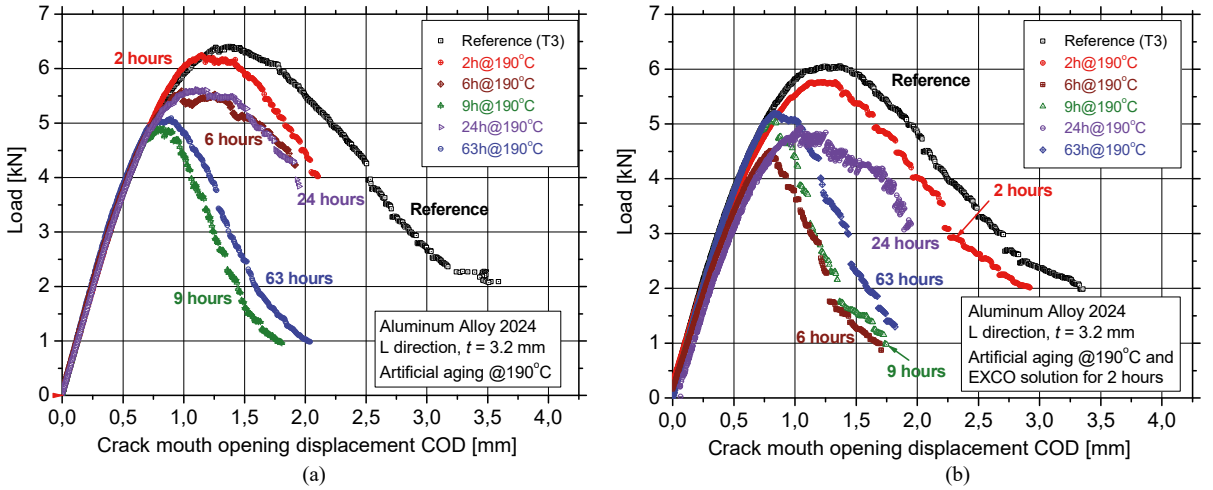

Fig. 2. Typical experimental resistance curves of (a) reference; (b) pre-corroded aluminum alloy 2024 specimens for different exposure times to exfoliation corrosion solution.

3.1.2. Elongation at fracture

The ductility results can be seen in Fig. 3 with solid black color line / filled triangles and dashed black line / hollow triangles for the aged and aged and corroded specimens, respectively. As we have used the logarithmic scale to express the artificial ageing time in hours, it is mathematically impossible to illustrate the reference condition T3 without any artificial ageing (zero hours of artificial ageing); to cope with this problem a very small value of 0.015 h was used in all Figures to address the reference specimens without any kind of artificial ageing heat treatment. The available experimental test results were simply interpolated with the aid of a B-Spline curve in order to roughly assess the effect of the two parameters: (a) ageing time and (b) ageing time and subsequent exposure to the corrosive solution.

For the case of the T3 condition (as-received) the ductility decrease due to corrosion exposure exceeds 26 %. As already discussed in previous section, no major corrosion-induced surface pits were formed that could act as stress raisers and therefore degrade the mechanical properties of the specimens. Hence, this ductility decrease is mainly attributed to the hydrogen embrittlement effect. For higher ageing times, e.g. in the peak-ageing condition, lower ductility decrease is noticed; almost 14 % (average) elongation at fracture decrease is evident for the peak-aged specimens, clearly showing that the fracture mechanism (embrittlement) has changed. For even higher ageing times (over-ageing condition) the corrosion-induced degradation changed again as the ductility decrease was “restored” at the order of magnitude around 18 %.

3.1.3. Critical stress intensity factor

The evaluation of the resistance curves for the different aging conditions and common 2 h exposure to the exfoliation corrosion solution of AA2024 has been made with the compliance method and according to the ASTM

E561 standard. The effective crack length values of the specimen were calculated from the COD values of the experiment, while the stress intensity K values were calculated from the force P values. The results of the calculations of the critical stress intensity factor values K_{cr} for the different artificial aging conditions of AA2024 and subsequent 2 h exposure to exfoliation corrosion solution can be seen in Fig. 3 (shown in the blue right y-axis) of the aged specimens (blue solid line and filled squares) against the respective aged and corroded specimens (dashed blue colour line and hollow squares) for the 190ºC artificial ageing temperature. All presented K_{cr} values have been calculated based on the nominal thickness t = 3.2 mm of the alloy. Marked in the diagram are the regions of under- peak- and over-ageing conditions as a function of time with different colors.

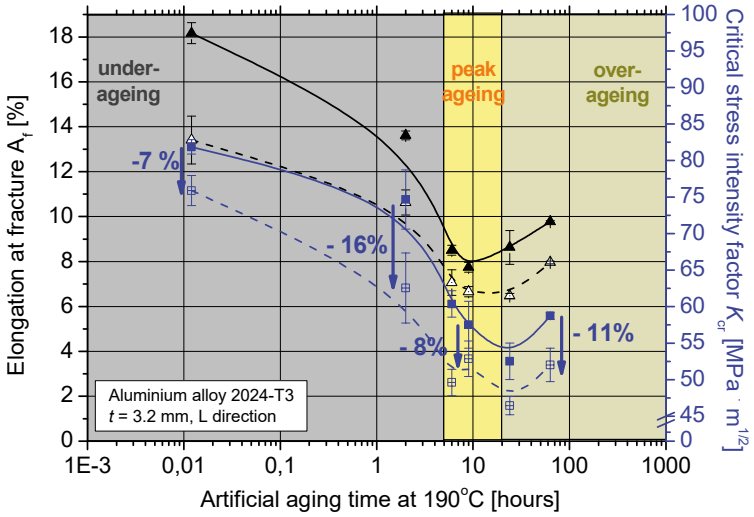

Fig. 3. Effect of 2 h EXCO exposure time to elongation at fracture as well as critical stress intensity factor for different artificial ageing conditions of aluminum alloy 2024.

The non-artificially aged material exhibited a fracture toughness value of 82 MPa√m, while after 2 hours exposure its fracture toughness value was decreased by approximate 7.5 % (76 MPa√m). For higher artificial ageing times, the effect of corrosion exposure seems to have a slightly higher decrease on fracture toughness; the K_{cr} decrease due to corrosion seems to be higher at the latest stages of under-ageing (approximately 16 % decrease). At the peak-ageing condition, the corrosion-induced decrease seems to be minimal (ranging from 4 to 8 %), while it is at the same order of magnitude (~ 7 to 11 % decrease) for the case of over-ageing condition. The trend of the corrosion-induced ductility decrease seems to be approximately the same with the K_{cr} decrease, for example maximum corrosion-induced decrease in the under-ageing regime, a shift to minimum decrease in the peak-ageing regime, while K_{cr} decrease seems to increase again with the over-ageing condition.

3.2. Discussion

From the previous section, it is evident that that AA2024 is very sensitive regarding its corrosion-induced fracture toughness degradation for the different aging conditions. Summing up all available results, the corrosion-induced percentage decrease has been calculated in Fig. 4. For the case of yield stress, it is evident that for all investigated artificial ageing conditions, the corrosion-induced decrease fluctuates around 5 % and no major increase/decrease can be noticed regarding the ageing condition of the alloy. An essential change of the tensile ductility A_f percentage decrease is noticed with the varying investigated ageing conditions. The results show that from the essential loss in ductility for the case of under-ageing condition (or T3), in the peak-ageing condition this decrease is minimum. This can be correlated with the precipitation sequence of the *S*-type phases along with the nucleation and growth kinetics of the precipitates. Finally, over-ageing condition seems to “restore” the high corrosion-induced decrease to the order of magnitude of the T3 condition. This was also associated with the coarsening of the precipitates that result in lesser number and higher diameter *S*-type precipitates.

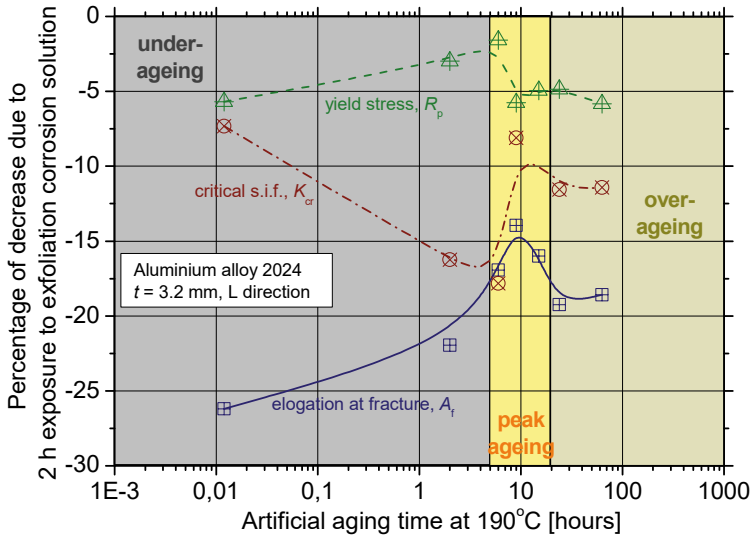

Fig. 4. Percentage corrosion-induced degradation of investigated mechanical properties of aluminum alloy 2024 for various artificial ageing conditions.

Corrosion-induced decrease on critical stress intensity factor seems to have an opposite trend than tensile ductility; K_{cr} is highly decreased within the over-ageing condition, exhibiting a local under-peak that has double or even triple percentage decrease that the starting, T3 condition. This of course should be correlated again with the precipitation sequence of the *S*-type phase, where the *GPB* zones are being precipitated in this regime. Within the peak-ageing regime, an inverse trend than A_f decrease is noticed. Critical stress intensity factor decrease is essentially lower within this regime, exhibiting local peaks of lower than 5 % decrease. This is in conjunction with the tensile ductility results, where the lowest corrosion-induced decrease was noticed in the same regime. In the over-ageing condition this decrease takes slightly higher values than the previous ageing condition (partial restoration again) and this was attributed to the precipitates coarsening, again. For the case of very extreme over-ageing condition (e.g. unpublished data from ageing temperature at 210°C), K_{cr} decrease is almost 2 % thus showing that the corrosion-induced decrease on the very long run is almost negligible.

3.3. Fractography

The tensile test results revealed that corrosion-induced ductility decrease is artificial-ageing sensitive; hence specimens from under-, peak- and over-ageing conditions were examined with the aid of scanning electron microscope (SEM). Fig. 4 shows SEM images for various ageing conditions and subsequent 2 hours corrosion exposure. Fig. 4a shows an image of a magnification of the fractured area; corrosion products with varying depth can be seen and below them steep surfaces are observed that is evidence of quasi-cleavage fracture mechanism corresponding to hydrogen embrittlement. In the smooth surfaces, dimples can be observed that were smaller in comparison with those observed in the center of the tensile specimen. The size of the dimples increased with increasing distance from the external surface of the sample, as also pointed out in Larignon et al (2013). This could be related to hydrogen embrittlement of the strengthening precipitates and/or interface matrix/precipitates.

Fig. 4b shows a respective image of a peak-aged specimen, subsequently corroded and strained till fracture. The corroded surface can be clearly seen; the corrosion-induced attack was uniform and localized embrittlement below the corrosion products (at the centre of the picture) can be distinguished. The fracture mode seems to be the classical void-coalescence due to the large plastic strains but definitely not exhibiting such high plastic strains as the previous specimen. Fig. 4c shows the respective picture for an overaged specimen, corroded and subsequently tensile strained till fracture. The corrosion products seems to be very uniform and small regions below the corrosion products exhibit a quasi-cleavage fracture mechanism, e.g. at the bottom left and upper left regions. This quasi-cleavage fracture mechanism was associated in Kamoutsi et al. (2006) with the hydrogen embrittlement mechanism. The rest

regions of the fracture surface exhibit large dimples that are denoting large plastic deformation before final fracture.

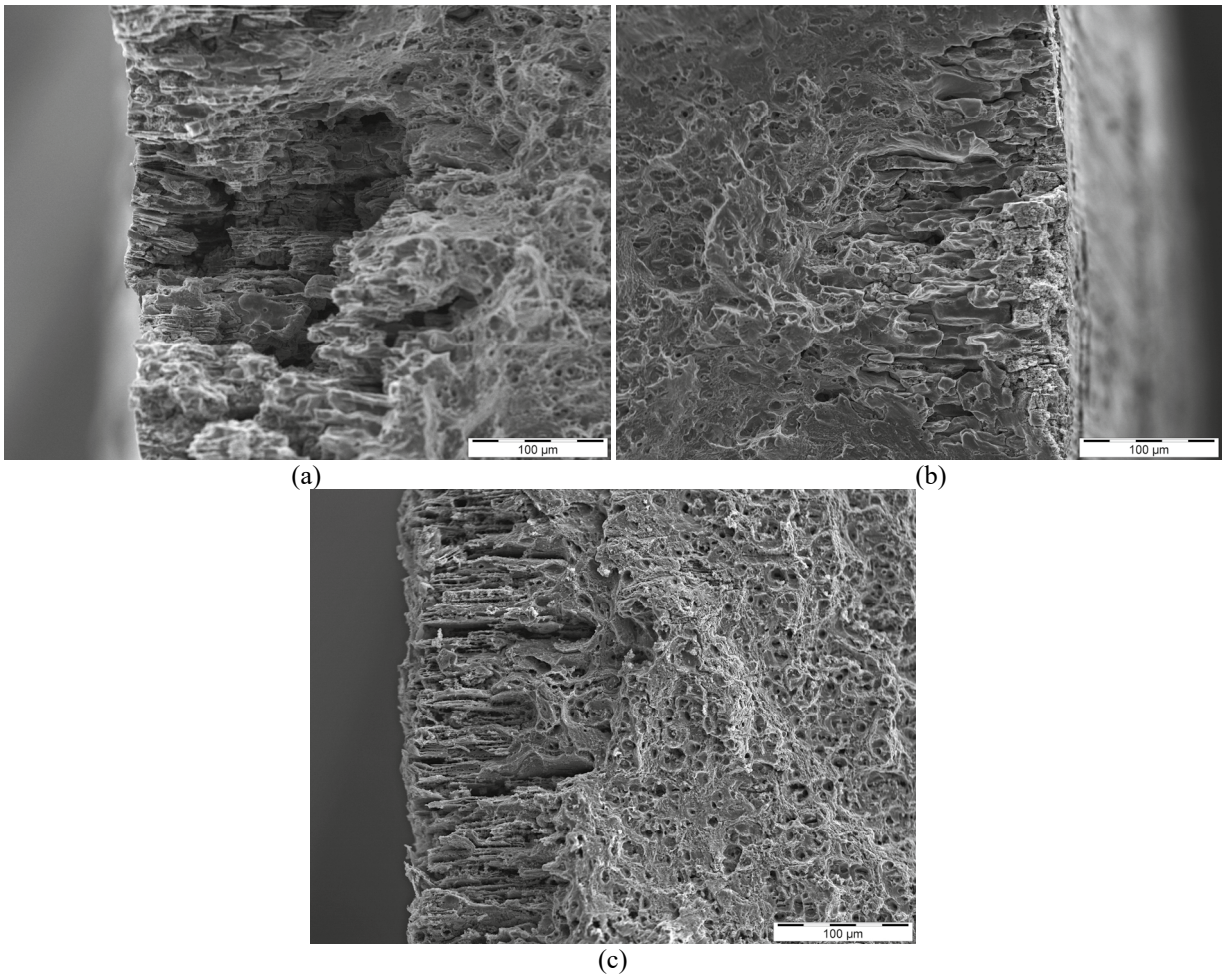

Fig. 4. Fracture surfaces of AA2024 tensile specimens for different artificially ageing conditions: at (a) under-ageing; (b) peak-ageing; (c) over-ageing when pre-corroded for 2 h exposure to EXCO solution.

4. Conclusions

Elongation at fracture and critical stress intensity factor seems generally to have the same trend regarding their corrosion-induced decrease that was absolutely dependant on the formation of *S*-phase precipitates. Exception is the under-ageing condition, where the formation GPB zones doubled or tripled the K_{cr} decrease, while the opposite was noticed for the A_f decrease. The lowest K_{cr} decrease (< 6 %) was noticed for the specimens at the peak-ageing condition (with formed *S´´* and *S´* precipitates) that also exhibited the lowest ductility decrease (~ 13 %) due to the corrosion exposure. At the over-ageing condition the corrosion-induced decrease was partially 'restored' at the T3 starting decrease level (~ 7 %) and even higher, while extreme artificial ageing leads to no significant corrosion-effect on the critical stress intensity factor.

Acknowledgements

The authors would also like to thank Carsten Blawert, Volker Heitmann and Petra Fischer at the Institute of Materials Research, Corrosion and Surface Technology of Helmholtz Zentrum Geesthacht, Germany for the

microstructure, fracture surface analysis of corroded specimens and fruitful discussions on the manuscript.

References

Alexopoulos, N.D., Papanikos, P., 2008. Experimental and theoretical studies of corrosion-induced mechanical properties degradation of aircraft 2024 aluminum alloy, Materials Science and Engineering, A498, 248-258.

Alexopoulos, N.D., Velonaki, Z., Stergiou, C.I., Kourkoulis, S.K., 2016. The effect of artificial ageing heat treatments on the corrosion-induced hydrogen embrittlement of 2024 (Al–Cu) aluminium alloy, Corrosion Science, 10, 413-424.

Bagaryatsky, Y.A. "Structural changes on Aging Al-Cu-Mg alloys", Dokl Akad SSSR 87 (1952) 397-559.

Boag, A., Hughes, A.E., Wilson, N.C., Torpy, A., MacRae, C.M., Glenn, A.M., Muster, T.H., 2009. How complex is the microstructure of AA2024-T3?, Corrosion Science, 51, 1565-1568.

Buchheit, R.G., Grant, R.P., Hlava, P.F., Mckenzie, B., Zender, G.L., 1997. Local dissolution phenomena associated with S phase (Al2CuMg) particles in aluminum alloy 2024-T3, Journal of the Electrochemical Society 144, 2621-2628.

Kamoutsi, H., Haidemenopoulos, G.N., Bontozoglou, V., Pantelakis, S.G., 2006. Corrosion-induced hydrogen embrittlement in aluminium alloy 2024, Corrosion Science 48, 1209-1216.

Larignon, C., Alexis, J., Andrieu, E., Odemer, G., Blanc, C., 2013. The contribution of hydrogen to the corrosion of 2024 aluminum alloy exposed to thermal and environmental cycling in chloride media, Corrosion Science 69, 211-220.

Mondolfo, L.F., "Aluminum alloys – structure and properties", London: Butterworth, 1976.

Ringer, S.P. Hono, K., Polmear, I.J., Sakurai, T., 1996. Nucleation of precipitates in aged Al-Cu-Mg-(Ag) alloys with high Cu:Mg ratios, Acta Materialia 44, 1883-1898.

Ringer, S.P., Caraher, S.K., Polmear, I.J., 1998. Response to comments on cluster hardening in an aged Al-Cu-Mg alloy, Scripta Materialia 39, 1559-1567.